2005 WHOI/NOAA Stratus2005
Field Program on the NOAA Ship Ronald H. Brown
October 5 – October 20, 2005
Results from the ETL Cloud and Flux Group and University of Miami Measurements

C. W. Fairall, E. F. Bradley, Sergio Pezoa, Ludovic Bariteau, Jessica Lundquist, Virendra Ghate
NOAA Environmental Technology Laboratory
Boulder, CO USA
October 22, 2005

1. Background on Measurement Systems

The ETL air-sea flux and cloud group conducted measurements of fluxes and near-surface bulk meteorology during the fall field program to recover the WHOI Ocean Reference Station buoy at 20 S Latitude 85 W Longitude. The ETL flux system was installed initially at Woods Hole, MA, in September 2005, shaken down on a three-day test cruise from WHOI to Charleston, and brought back into full operation in Panama in late September, 2005. The air-sea flux system consists of six components: (1) A fast turbulence system with ship motion corrections mounted on the jackstaff. The jackstaff sensors are: INUSA Sonic anemometer, OPHIR IR-2000 IR-hygrometer, LiCor LI-7500 fast CO_2/hygrometer, and a Systron-Donner motion-pak. (2) A mean T/RH sensor in an aspirator on the jackstaff. (3) Solar and IR radiometers (Eppley pyranometers and pyrgeometer) mounted on top of a seatainer on the 02 deck. (4) A near surface sea surface temperature sensor consisting of a floating thermistor deployed off port side with outrigger. (5) A Riegl laser rangefinder wave gauge mounted on the bow tower. (6) An optical rain gauge mounted on the bow tower. Slow mean data (T/RH, PIR/PSP, etc) are digitized on a Campbell 23x datalogger and transmitted via RS-232 as 1-minute averages. A central data acquisition computer logs all sources of data via RS-232 digital transmission:

1. Sonic Anemometer
2. Licor CO2/H2O
3. Slow means (Campbell 21x)
4. Laser wave sensor
5. OPHIR hygrometer
6. Systron-Donner Motion-Pak
7. Ship's SCS
8. ETL GPS

The 8 data sources are archived at full time resolution. At sea we run a set of programs each day for preliminary data analysis and quality control. As part of this process, we produce a quick-look ascii file that is a summary of fluxes and means. The data in this file come from three sources: The ETL sonic anemometer (acquired at 21.3 Hz), the ship's SCS system (acquired at 2 sec intervals), and the ETL mean measurement systems (sampled at 10 sec and averaged to 1 min). The sonic is 5 channels of data; the SCS file is 15 channels, and the ETL mean system is 42 channels. A series of programs are run that read these data files, decode them, and write daily text files at 1 min time resolution. A second set of programs reads the daily 1-min text files, time

matches the three data sources, averages them to 5 or 30 minutes, computes fluxes, and writes new daily flux files. The 5-min daily flux files have been combined and rewritten as a single file to form the file *flux_5hf_stratus_05.txt*. The 1-min daily ascii files are stored as *proc_nam_dayDDD.txt* (nam='pc', 'scs', or 'son'; DDD=yearday where 000 GMT January 1, 2005 =1.00). File structure is described in the original matlab files that write the data, *prt_nam_05.m*.

Atmospheric aerosols were measured with a Particle Measurement Systems (PMS) Lasair-II aerosol spectrometer. The Lasair-II draws air through an intake and uses scatter of laser light from individual particles to determine the size. Particles are counted in six size bins: 0.1-0.2, 0.2-0.3, 0.3-0.5, 0.5-1, 1-5, and greater than 5.0 μm diameter. The ETL system was mounted in the seatainer on the 02 deck with the intake on the upwind side of the container. The system ran at 1.0 cfm (0.028 m3/min) sample volume flow rate with a count deconcentrator that reduces the counts a factor of 10 (to prevent coincidence errors).

ETL/Flux and UM also operated six remote systems: a Vaisala CT-25K cloud base ceilometer, a 9.4 GHz vertically pointed Doppler cloud radar, a 915 MHz Doppler wind profiler, and three microwave radiometer systems. The RHB's scanning Doppler C-band radar was not operated because of a transmitter failure. The ceilometer is a vertically pointing lidar that determines the height of cloud bottoms from time-of-flight of the backscatter return from the cloud. The time resolution is 30 seconds and the vertical resolution is 15 m. The raw backscatter profile and cloud base height information deduced from the instrument's internal algorithm are stored in daily files with the naming convention *CRVYYDDD.raw* where YY=04 and DDD=julian day. File structure is described in *ceilo_readme_stratus04.txt*.

ETL/Flux and UM used an integrated system in a seatainer that includes the 3-channel microwave radiometer (20.6-31.65-90.0 GHz Mark II unit). The UM 9.4-GHz radar antenna was mounted on the roof of the seatainer. The cloud radar systems can be used to deduce profiles of cloud droplet size, number concentration, liquid water concentration, etc. in stratus clouds. If drizzle (i.e., droplets of radius greater than about 50 μm) is present in significant amounts, then the microphysical properties of the drizzle can be obtained from the first three moments of the Doppler spectrum. Two Radiometrics Inc. 'Mailbox' microwave radiometers were also deployed. The Old unit is the same one that has been deployed on numerous TAO/PACS cruises and on EPIC2001. For the first time, we brought a new Mailbox unit just acquired in September. This unit is destined for an Arctic project but the schedule allowed it to be used on this cruise. The new unit does continuous tip curves and produces profiles of water vapor distribution.

For the record, five or six times a day photographs have been taken of the sky in four directions relative to the ship (over starboard, astern, port, and bow), especially at times of rapid cloud development. The timing of each set of four photographs has been carefully noted so that the directions can be converted to earth coordinates, knowing the ship's heading at that time.

2. Selected Samples

a. Flux Data

Preliminary flux data is shown for yearday=286 (October 13, 2005) as the RHB remains on station at the buoy site at 20 S 85 W (Fig. 1.). The time series of ocean and air temperature is given in Fig. 2. The water temperature is about 18.5 C and the air temperature is about 17.0 C.

The apparent increase in air temperature near the end of the day is caused by the ship turning downwind. The true wind direction (Fig. 3) and true wind speed (Fig. 4) show modulation by boundary-layer scale organization. The effect of clouds on the downward solar flux is shown in Fig. 5 and on the IR flux in Fig. 6. For the solar flux, broken clouds are apparent in the jagged form of the curve during the morning. For IR flux, clear skies have values of about 320 Wm^{-2} and cloudy skies values around 390 Wm^{-2}. The IR flux and solar flux show a large break in the clouds in the afternoon. Fig. 7 shows the time series of four of the five primary components of the surface heat balance of the ocean (solar flux is left out). The largest term is the latent heat (evaporation) flux, followed by the net IR flux (downward minus upward); the sensible heat flux and the flux carried by precipitation are very small. We are using the meteorological sign convention for the turbulent fluxes so all three fluxes actually cool the interface in this case. The time series of net heat flux to the ocean is shown in Fig. 8. The sum of the components in Fig. 7 is about -130 Wm^{-2}, which can be seen in the night time trace; the large positive peak during the day is due to the solar flux. The integral over the entire day gives an average flux of 61 Wm^{-2}, indicating strong warming of the ocean mixed layer even on an overcast day.

b. Remote Sensing Data

A sample ceilometer 24-hr time series for cloud base height for October 14 is shown in Fig. 9. This day had 83% cloud cover and two sets of cloud base heights: the dominant stratocumulus layer with cloud bases 1000 to 1300 m and occasional lower level 'scud' clouds with bases about 500 m. Small amounts of drizzle can be seen as the few low-altitude dots early in the day. A sample time-height cross section (Fig. 10) from the UM cloud radar is shown for a 24-hr period on October 14. The panels indicated the intensity of the return (upper), the mean fall velocity of the scattering droplets (middle panel), and the Doppler width of the return. This happens to be a day with low cloud cover; clouds are fairly thin with tops at 1.0 - 1.5 km. Light drizzle events are apparent as the light blue colors (2 m/s fall speed) in the mean Doppler panel; the radar is much more sensitive to drizzle than the ceilometer.

Time series from two of the microwave radiometers for day 285 (October 12) are shown in Fig. 11. The upper panel shows column integrated water vapor; the lower panel shows the integrated liquid water path (LWP) of the stratus clouds. The data are from the two Radiometrics mailbox radiometers (referred to as *new* and *old* units). The new unit was obtained for use in the Arctic and is presently using Arctic coefficients to retrieve vapor and liquid quantities. The two are highly correlated, but differ by a factor of 10 in liquid water. This will be sorted out when retrievals with the new system are done with appropriate coefficients.

A sample time series from the laser wave gauge is shown in Fig. 12. This device measures the range from a point on the mast to a point on the ocean. The distance includes the motions of the sea surface (waves) plus motion of the ship up and down relative to mean sea level. The ship motion component will be removed using motion correction data from the flux system.

The wind profiler operates at 33 cm wavelength where it is sensitive to enough to detect returns from turbulent variations in radar refractive index, principally associated with gradients in atmospheric moisture; it also sensitive to precipitation. Sensitivity to moisture gradients causes the marine inversion to show up clearly as a band of increased backscatter intensity. Both of these factors cause improved height performance in stormy conditions. During Stratus 2005

the profiler gave continuous retrievals of the boundary-layer wind profile through the inversion. Sea clutter tends to invalidate the winds at heights below 500 m, although the minimum usable height depends on the amount of whitecapping, sea state, the dryness of the atmosphere, and ship operational factors (underway versus stopped, etc). A sample profiler wind is shown in Fig. 13 in comparison with the balloon sondes and the near-surface observations from the ship. Winds in the boundary layer are predominately from the SE.

3. Cruise Summary Results

a. Basic Time Series

The ship track for the entire cruise is shown in Fig. 14. The 5-min time resolution time series for sea/air temperature are shown in Fig. 15 and for wind speed and N/E components in Fig.16. The change in conditions for the first five days of the record is associated with the run south along 85 W from Panama. Then on day 291 we departed the WHOI location and moved toward the DART buoy at 20 S 74.8W. The near-surface sea-air temperature difference is about 1 C in the vicinity of the WHOI buoy. It increases to more than 2 C on days 284-285 during the drizzly and broken cloud phase. The mean diurnal cycle for the wind components (Fig. 17) shows a weak diurnal variation with a minimum at 1600 local time. Primarily because of the healthy wind speeds (about 9 m/s), there is only a small diurnal signal (0.10 C) in the sea surface temperature. Time series for flux quantities are shown as daily averages. Fig. 18 gives the flux components and Fig. 19 the cloud forcing for net surface radiative fluxes. Cloud forcing is the difference in the measured radiative flux from that which would be expected if there were no clouds. It is essentially a measure of the effect of clouds on the energy budget of the ocean. A negative cloud forcing implies the cloud cools the ocean (e.g., by reflecting solar flux).

The diurnal cycle of cloudiness (i.e., thinning or clearing after local noon) at 20 S leads to fairly large values of net heat flux and solar flux; afternoon clearing leads to much greater 24-hr average solar flux. Just for amusement, bulk meteorological variables and turbulent heat fluxes are shown for the transect from 0 S to 20 S along 85 W is shown in Fig. 20. This shows the winds peaking at 15 S with a maximum in latent heat flux at 125 W/m^2. The Eastern return transect (Fig. 21) looks similar to transects along 20 S in previous years.

Data from the PMS Lasair-II aerosol spectrometer is shown in Fig. 22. This instrument counts particles in size ranges from 0.1 to 5 μm diameter based on scattering of light from a laser beam. This size range includes most of the so-called accumulation-mode aerosols that represent most of the particles activated to form droplets in clouds. Thus, the total number of aerosols counted by this device is expected to correlate with cloud condensation nuclei and the number of cloud drops. The distribution is normally strongly bimodal as a result of cloud processing in the marine boundary layer. The Lasair-II only observes the large particle size mode. The concentration varies with a time scale of several days. This is the result of the complex interaction between entrainment, advection, production and scavenging of aerosols. The most interesting feature this year is the dramatic decrease that occurred on day 285. In 2004 the average total number concentration from December 8th to the 18th was 180 (cm^{-3}). In 2005, the median in the vicinity of the buoy was 85 (cm^{-3}).

b. Boundary Layer and Cloud Properties

Beginning at 0000 UTC on October 5 and ending at 2300 UTC on October 18 we completed 72 successful rawinsonde launches. While at the WHOI buoy sondes were launched 6 times daily; otherwise, they were launched 4 times daily. A time-height color contour plot of temperature is shown in the upper panel of Fig. 23; the lower panel shows the relative humidity. A pronounced temperature inversion is evident at approximately 1.2-1.6 km. The time series of wind speed and direction are shown in Fig. 24. The winds are consistent with climatology, with southeasterlies prevailing within the boundary layer and westerlies aloft. The nominal height for the transition from westerlies to easterlies descended steadily during the experiment in coincidence with the moisture transition described above. The boundary-layer inversion is more clearly seen in potential temperature (Fig. 25). Here the BL depth was initially about 1.0 km on the equator but was fairly constant at 1.4 km in the region of the buoy except for a clear diurnal cycle with a maximum about 1000 UTC.

The time series of cloud base height from the ceilometer is shown in Fig. 26. Three different microwave radiometer systems were used on the cruise. The microwave radiometers are calibrated using a tipcal process that requires clear skies. With the Mark II system, this is done manually. The 32 GHz channel of the Mark II misbehaved on the cruise. At this writing we don't know if it is a hardware problem or a gain drift (a gain drift would be cured by frequent tipcals). Several tipcals were done in port in Woods Hole, but during the cruise sky conditions did not permit new tipcals with the lone exception of day 284. The Radiometrics systems perform tipcals automatically: the old unit hourly and the new unit continuously. The time series of data from the two mailbox systems is shown in Fig. 27. Both systems agreed fairly well with sonde column water vapor values in the stratus region. The new system showed much higher correlation with the sondes than the old system, but the slope was not as close to 1.0 and it was biased high. This suggests that the scanning strategy of the new system gives much better sampling but there are still retrieval issues to solve.

4. Intercomparisons

Intercomparisons are a key strategy in data quality assurance for the climate reference buoys and the use of research vessel measurements for climate-quality data archives. The ETL flux system is intended to produce measurements of turbulent flux bulk variables and radiative fluxes that have the required accuracy for climate research. For this cruise, a set of Intercomparisons were done for bulk meteorology and radiative fluxes.

*The ETL flux system acquired all relevant ship IMET-based measurements.
*ETL and ship radiative fluxes were compared with the WHOI buoy (sitting on the deck) and an array of IMET radiative sensors (mounted in an array on the 03 deck).
*A carefully executed set of psychrometer measurements were taken regularly during the cruise as a reference for air temperature and humidity.

a. ETL-Ship Comparisons

We compared ETL and ship measurements for wind speed and direction, water and air temperature, relative humidity, and solar and IR downward radiative flux. All measurements agreed within the accuracy required for flux evaluations. The ship wind system does experience

flow blockage by the jackstaff for relative winds from the starboard side. A detailed analysis will be done later.

b. Psychrometer Comparisons

As in some previous cruises, the accuracy of our Vaisala temperature and humidity measurements was checked against a hand-held Assman psychrometer. About 5 times throughout the day, when the wind was within ±90º of dead ahead, the Assman wet and dry bulb temperatures were sampled through either port or starboard chocks on the foredeck. These locations were adopted on earlier cruises, rather than over the bow itself, because they offer shading of the thermometers from the sun. The chocks are at a height of approximately 7.5 meters above the sea surface, compared with 15m for the Vaisala. A sample calculation based on the z/L value indicated that the temperature correction with height would be around 0.03ºC. This is less than the resolution with which the thermometers can be read (0.1ºC). These are spot values to be compared with our standard 5-minute averages, so some scatter is expected, but averaged over the cruise the comparison should be valid.

ETL, ship, and psychrometer values were compared for air temperature and specific humidity. The 7.5-meter psychrometer values were corrected to 15 m using similarity theory (based on the measured fluxes). The average correction was -0.02 C for temperature and -0.12 g/kg for humidity. The results for 62 samples are shown as scatter plots in Figs. 28 and 29; means are summarized in the table of mean values and standard deviations of differences given below:

	Mean ETL	Mean Ship	Mean Psy	Ensemble	$\sigma_{ETL\text{-}ship}$	$\sigma_{ETL\text{-}Pshch}$
T_{air} (C)	17.51	17.32	17.54	**17.45**	0.03	0.15
Q_{air} (g/kg)	9.00	8.96	8.89	**8.95**	0.05	0.21

The differences in humidity (0.04 g/kg) in ETL and ship values are too small to be resolved by the psychrometer (accurate on average to 0.1 C and 0.1 g/kg). For temperature, the psychrometer agrees with the ETL sensor. All three sensors are within required accuracy (0.2 C or g/kg) of the ensemble mean.

5. ETL Data Cruise Archive

Selected data products and some raw data were made available at the end of the cruise for the joint cruise archive. Some systems (radar, turbulence, microwave radiometer) generate too extravagantly to be practical to share. Compared to processed information, the raw data is of little use for most people. For the cloud radar we have made available image files only; full digital data will be available later from the ETL website. For the microwave radiometers, the time series after some processing and averaging. No direct turbulent flux information is provided; that will be available after re-processing is done back in Boulder. However, bulk fluxes are available in the flux summary file

Data Archive Directories

Ceilo	Ceilometer files (processed file, images)
Flux	Air-sea flux files (processed flux files: daily files, cruise file, some m-files)
Sondes	Rawindsone files (.EDT, .PTU, .WND)
Aerosol	Time series of aerosol concentration at different sizes
Microwv	Microwave radiometer files (processed files; graphic display)
X-Radar	Image files from U. Miami X-band cloud radar
Reports	Documentation (cruise report, summary image files)
UProf	Image and data files from the wind profiler
Pics	Powerpoint files of sky pictures

Contact:
C. Fairall
NOAA Environmental Technology Laboratory
325 Broadway
Boulder, CO USA 80305
303-497-3253
chris.fairall@noaa.gov

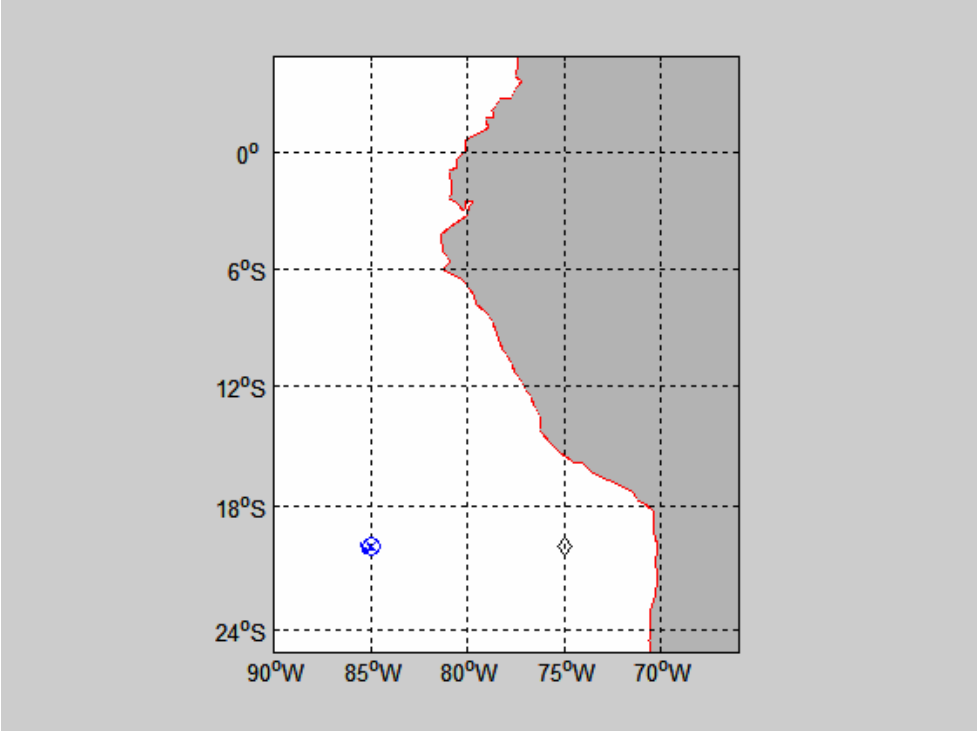

Figure 1. Cruise track for RBH on October 13 (DOY 286). The x marks the WHOI buoy location; the diamond is the DART buoy.

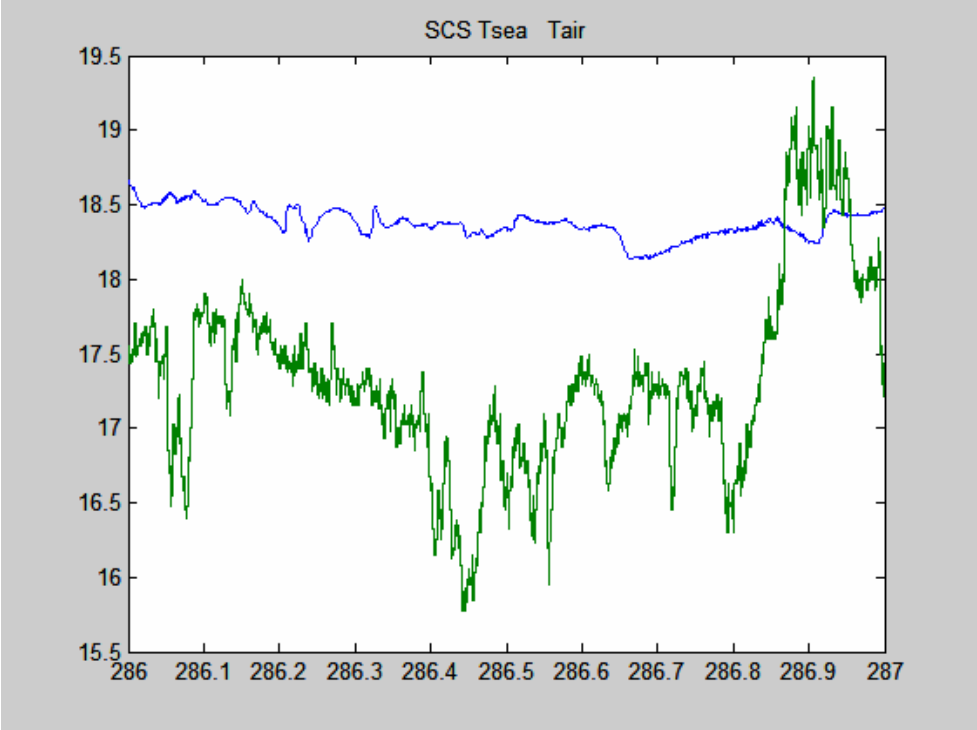

Figure 2. Time series of near-surface ocean temperature (green) and 15-m air temperature (blue).

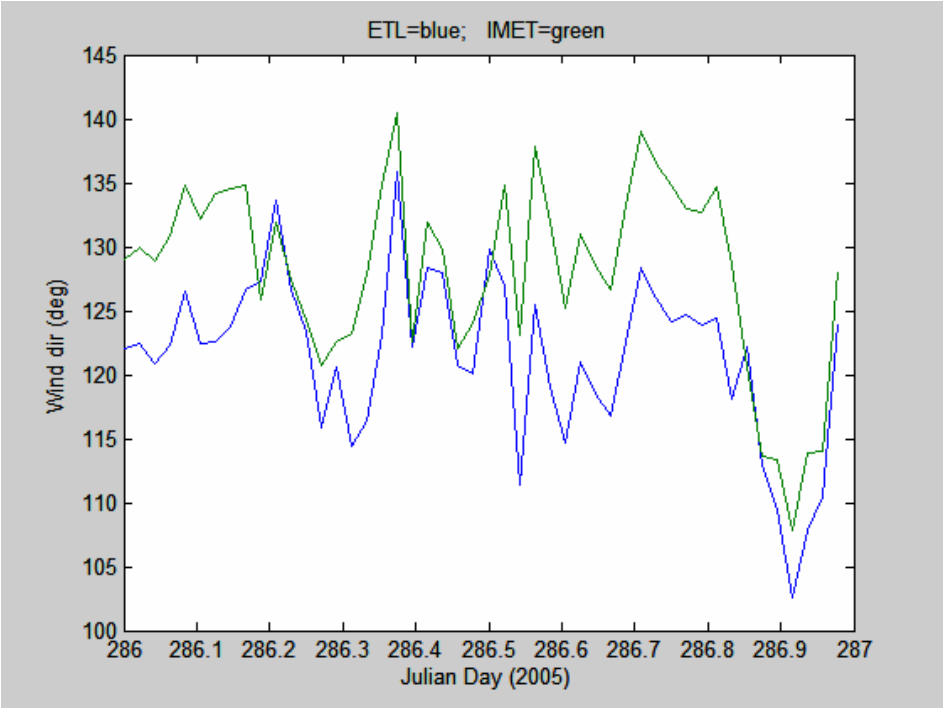

Figure 3. True wind direction from the ETL sonic anemometer (18 m) and the IMET propvane (15 m).

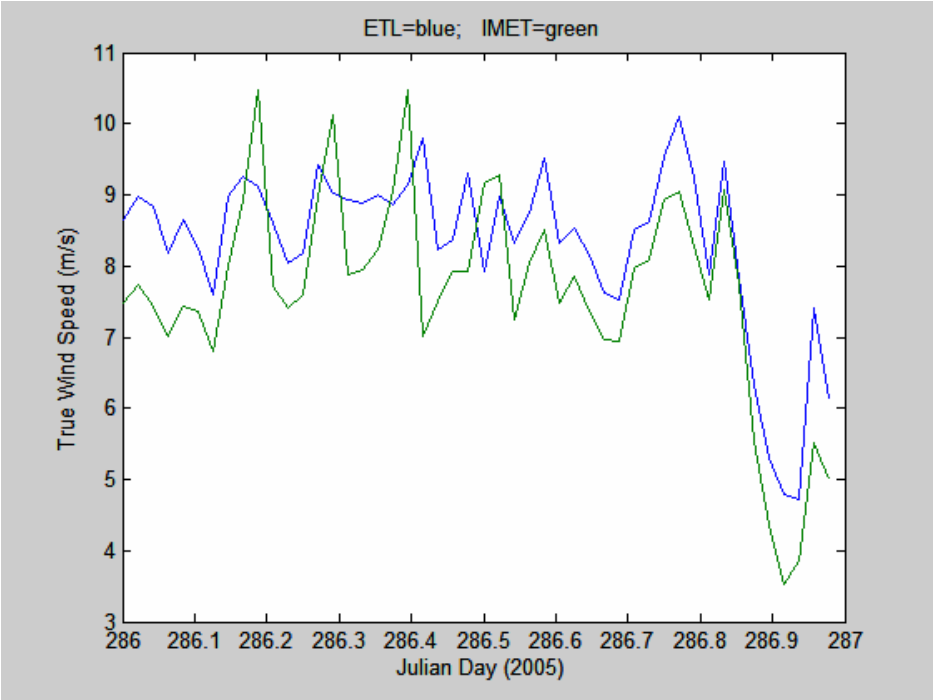

Figure 4. True wind speed from the ETL sonic anemometer (18 m) and the ship's propvane (15 m).

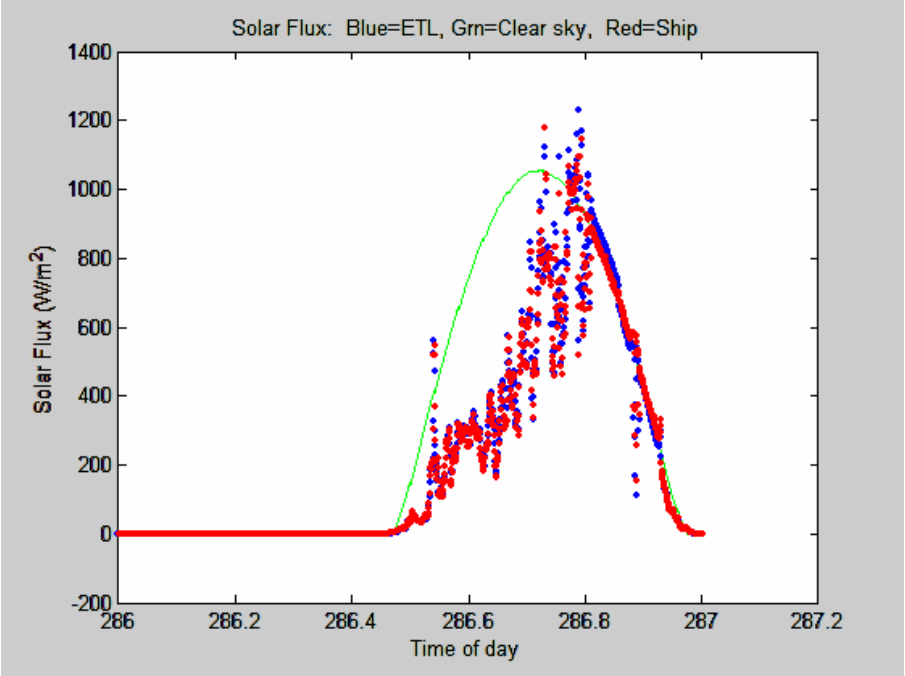

Figure 5. Time series of downward solar flux from ETL and ship Eppley sensors**.** The green line is a model of the expected clear sky value.

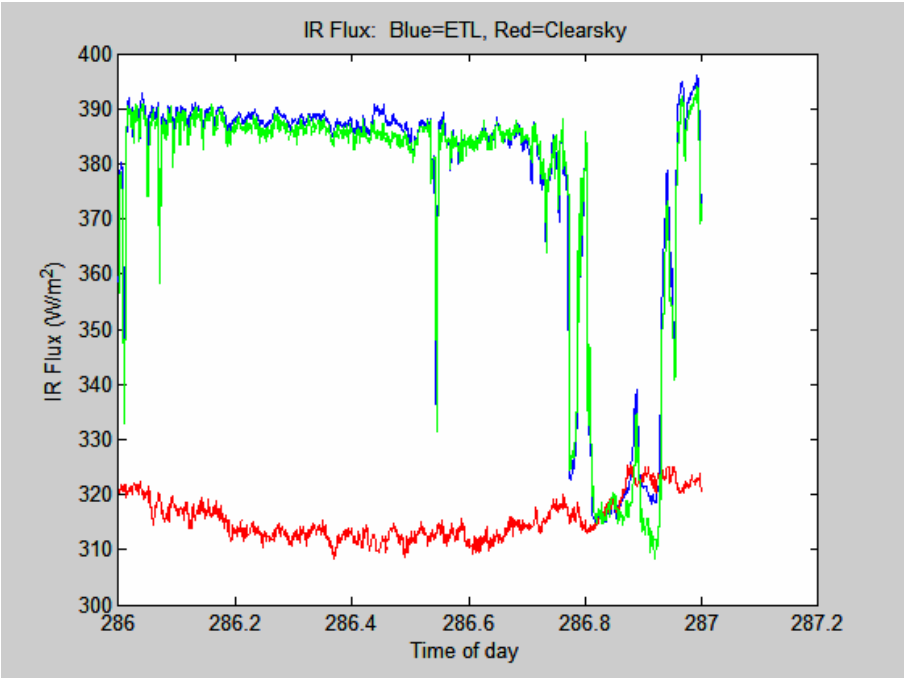

Figure 6. Time series of downward IR flux from ETL and ship Eppley sensors. The red line is a model of the expected clear sky value.

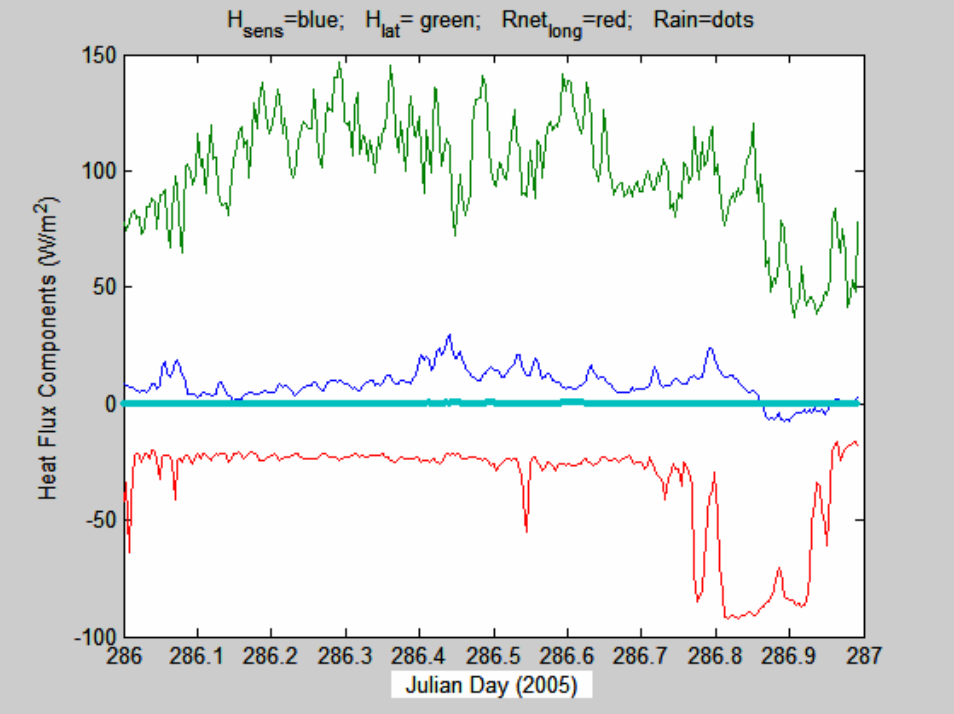

Figure 7. Time series of non-solar surface heat flux components: sensible (blue), latent (green), and net IR (red).

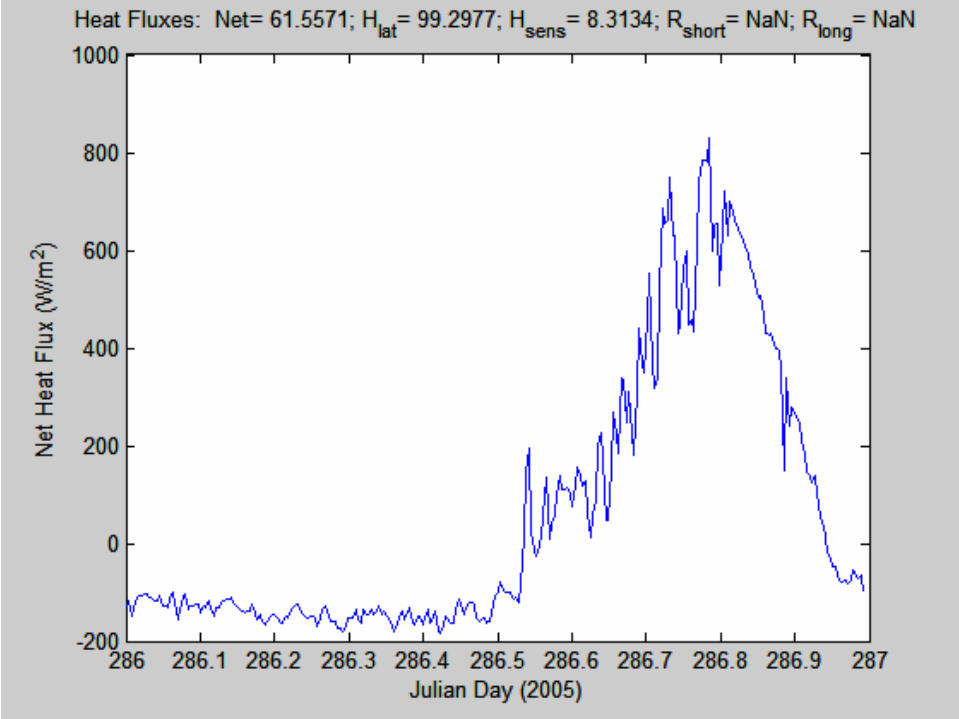

Figure 8. Time series of net heat flux to the ocean surface. The values at the top of the graph are the average for the day for each component of the flux.

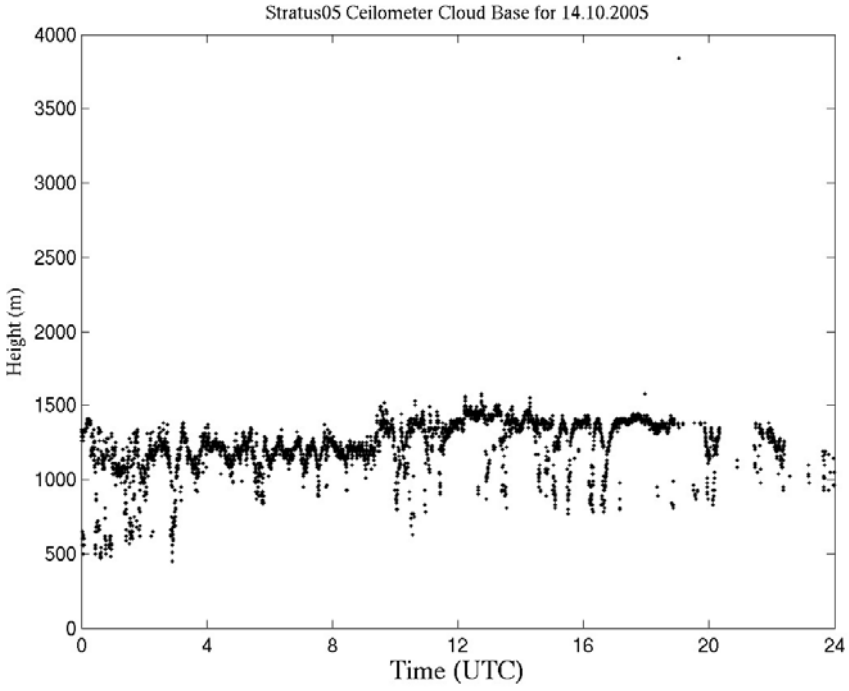

Figure 9. Cloud-base height information extracted from the ceilometer backscatter data for day 287 (October 14, 2005).

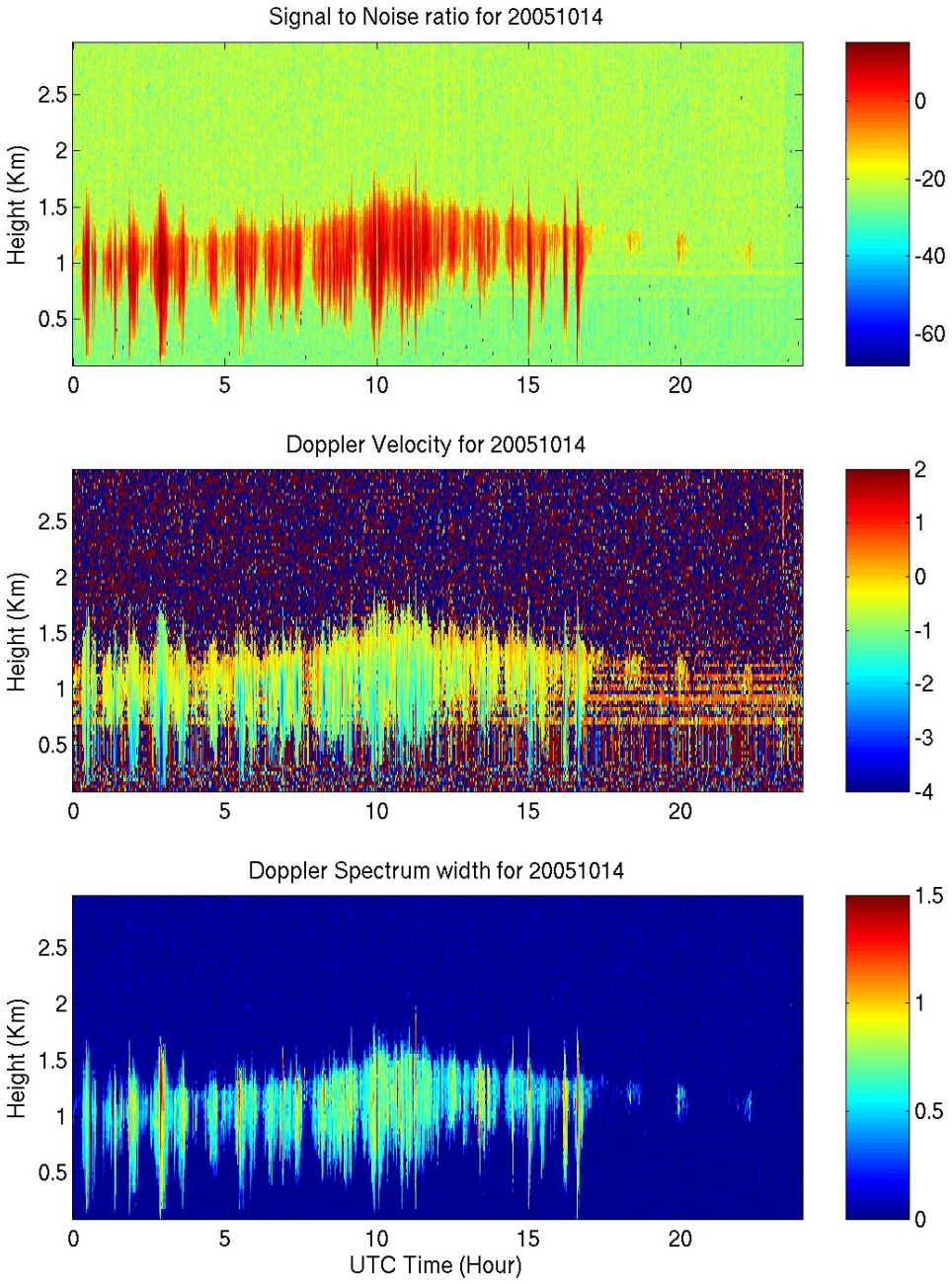

Figure 10. Time-height cross section data from 9.4 GHz cloud radar data for day 287 (October 14, 2005): upper panel, backscatter intensity; middle panel, mean Doppler vertical velocity; lower panel, Doppler width. The deep vertical streaks are drizzle.

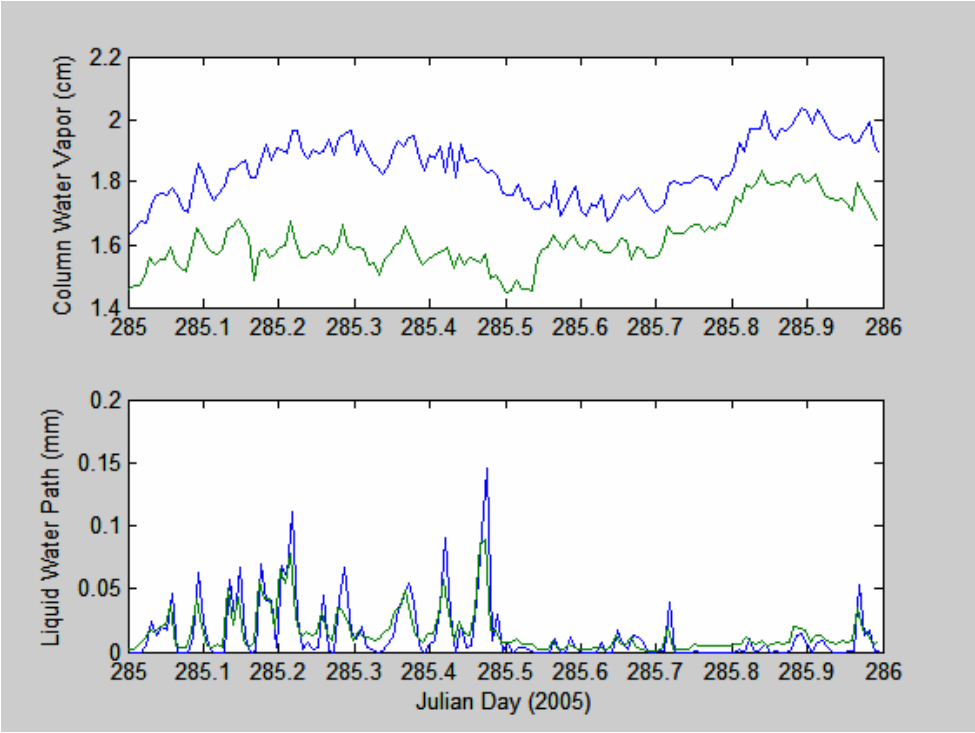

Figure 11. Time series of data from both the *new* and the *old* Radiometrics microwave radiometers: upper panel – column water vapor, lower panel – column water liquid. Note, new radiometer liquid water has been divided by 10.

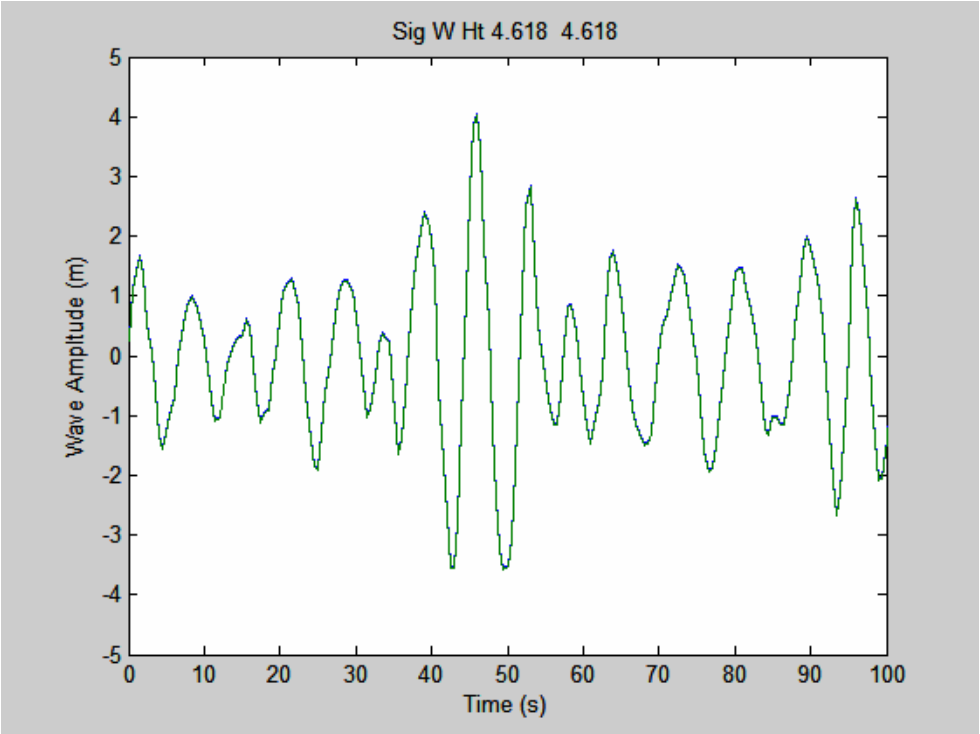

Figure 12. Sample wave time series from 1000 UTC on day 286 (October 13) from the laser rangefinder. The trace shows elevation of the sea surface relative to the bow of the ship. The dominant wave period is about 6 seconds.

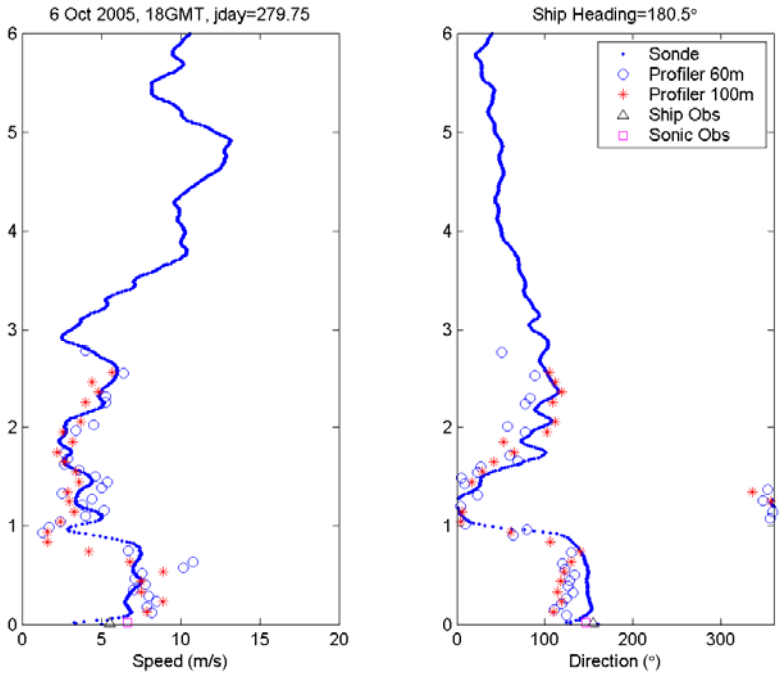

Figure 13. Wind speed and direction comparison of the wind profiler and the rawinsonde launched 18 Z October 6, 2005.

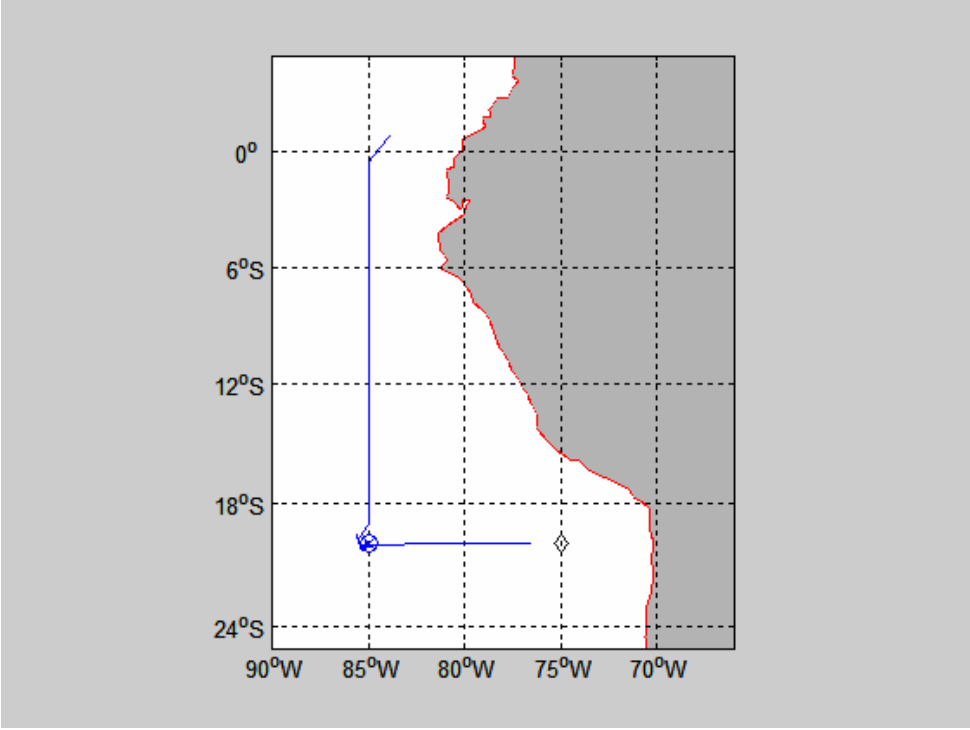

Figure 14. Cruise track for entire Stratus 2005 cruise.

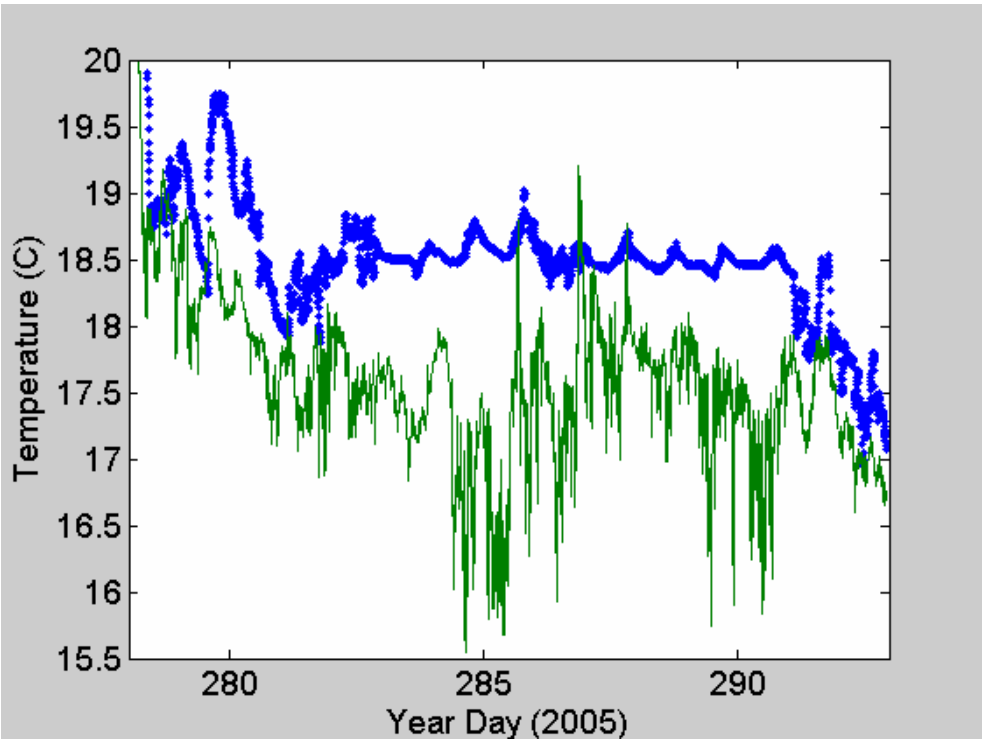

Figure 15 Time series of near-surface ocean temperature (blue) and 15-m air temperature (green) for the 2005 RHB Stratus cruise.

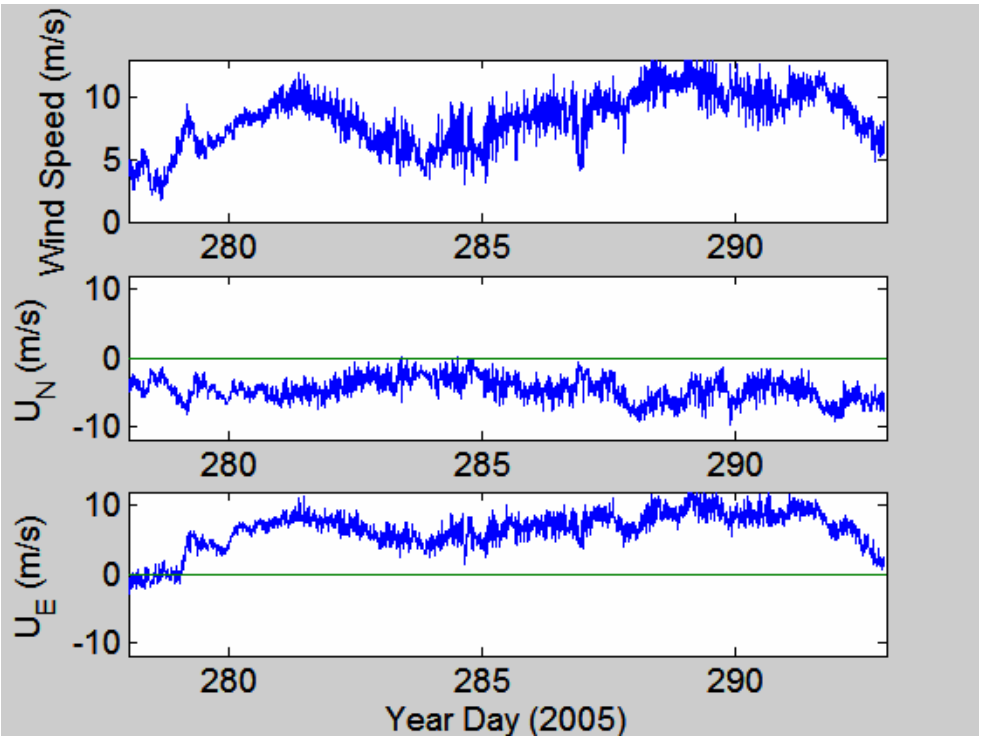

Figure 16. Time series of wind speed (upper panel), northerly component (middle panel), and easterly component (lower panel) for the 2005 RHB Stratus cruise.

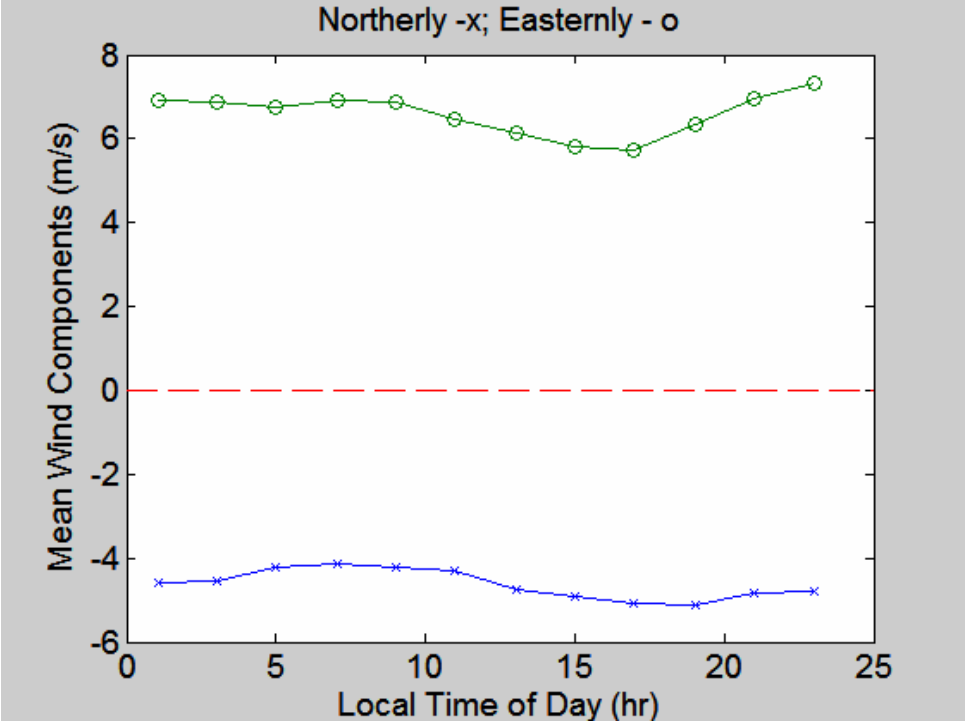

Figure 17. Diurnal average of northerly and easterly wind components for period near 20 S 85W.

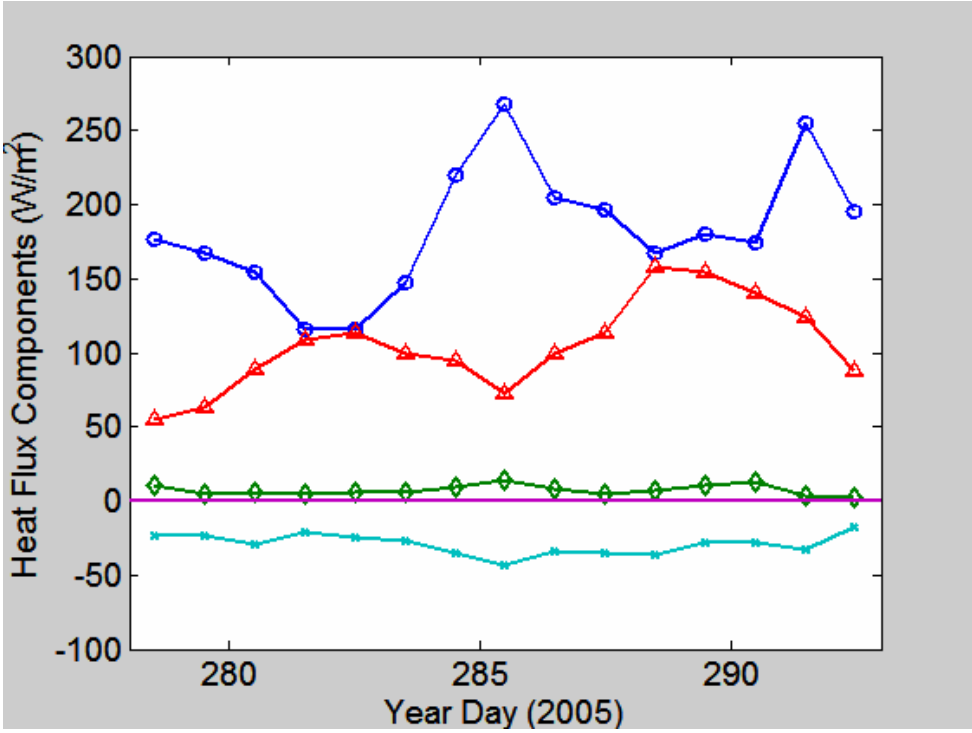

Figure 18. Time series of 24-hr average heat flux components: solar flux - circles; latent heat flux - triangles; sensible heat flux - diamonds; net IR flux x's.

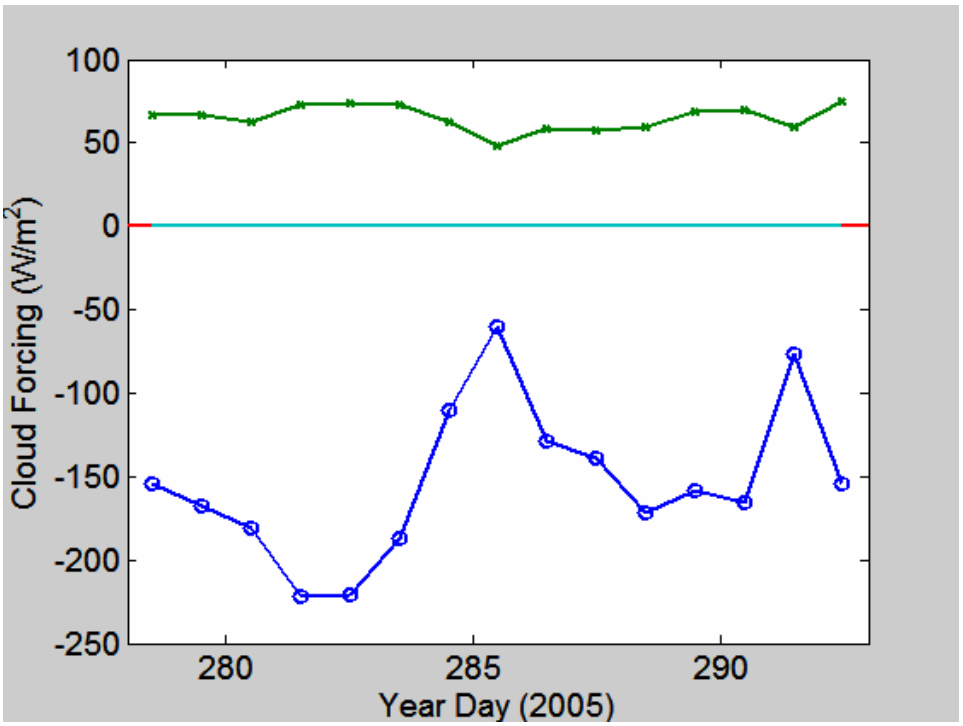

Figure 19. Time series of daily averaged radiative cloud forcing: IR CF (W/m^2) – green, Solar CF (W/m^2) – blue.

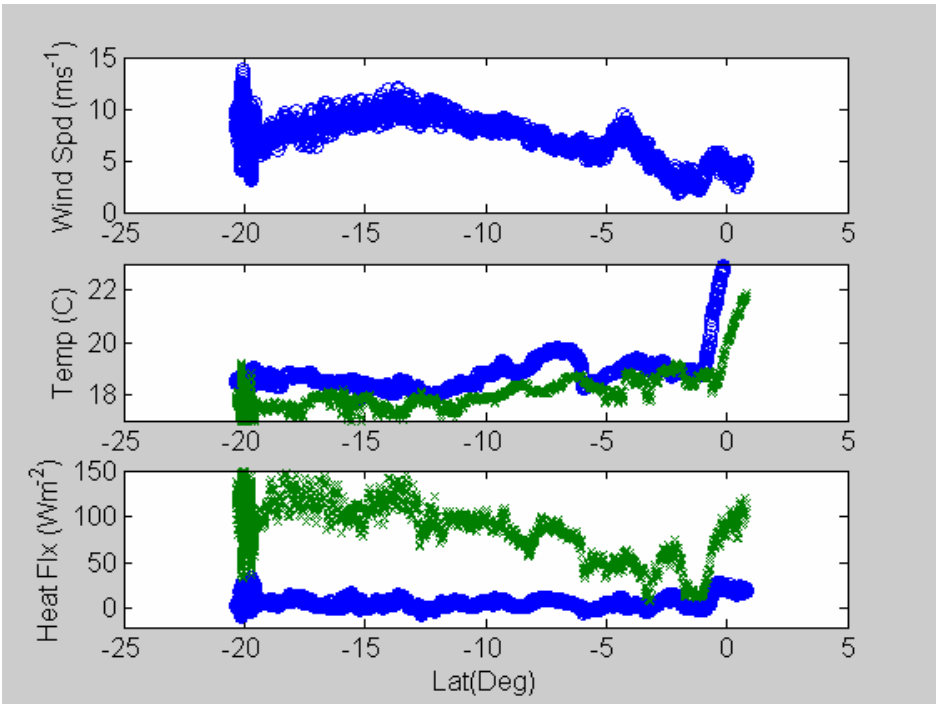

Figure 20. Selected variables from the N-S transect along 85 W. Upper panel is wind speed; the middle panel is sea surface temperature (blue) and air temperature (green); the lower panel shows sensible (blue) and latent (green) heat fluxes.

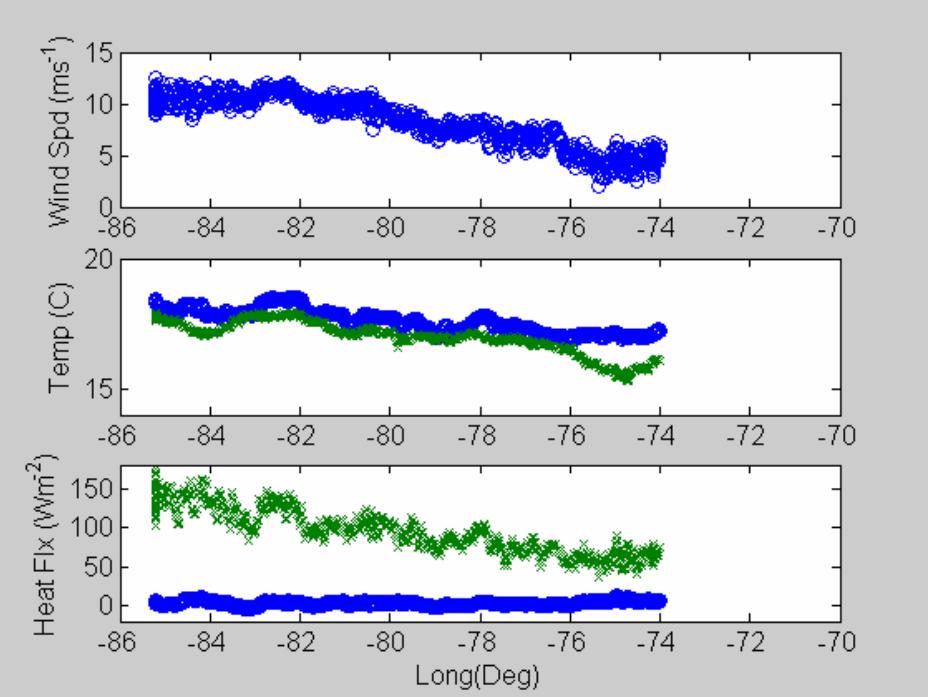

Figure 21. Same as Fig. 20, but for the W-E transect along 20 S from 85 W to 70 W.

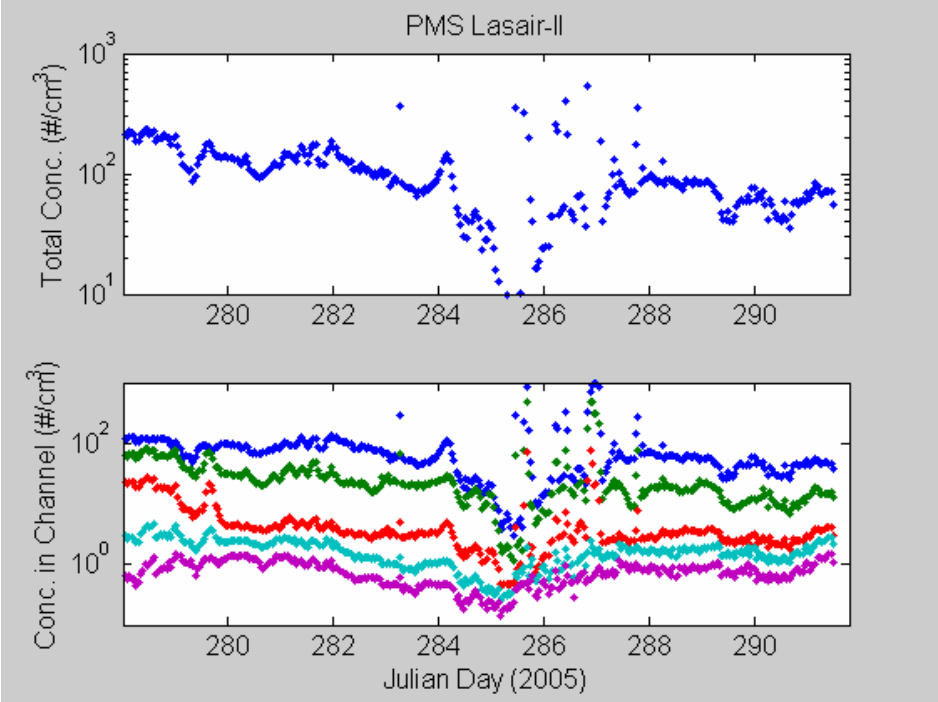

Figure 22. Aerosol concentrations from Lasair-II spectrometer. Upper panel: total number concentration for aerosols larger than 0.1 micron diameter. Lower panel: aerosol concentrations for 0.1-0.2 (blue), 0.2-0.3 (green), 0.3-0.5 (red), 0.5-1.0 (cyan), and 1.0-5.0 (magenta). Spikes are caused by the ship's exhaust.

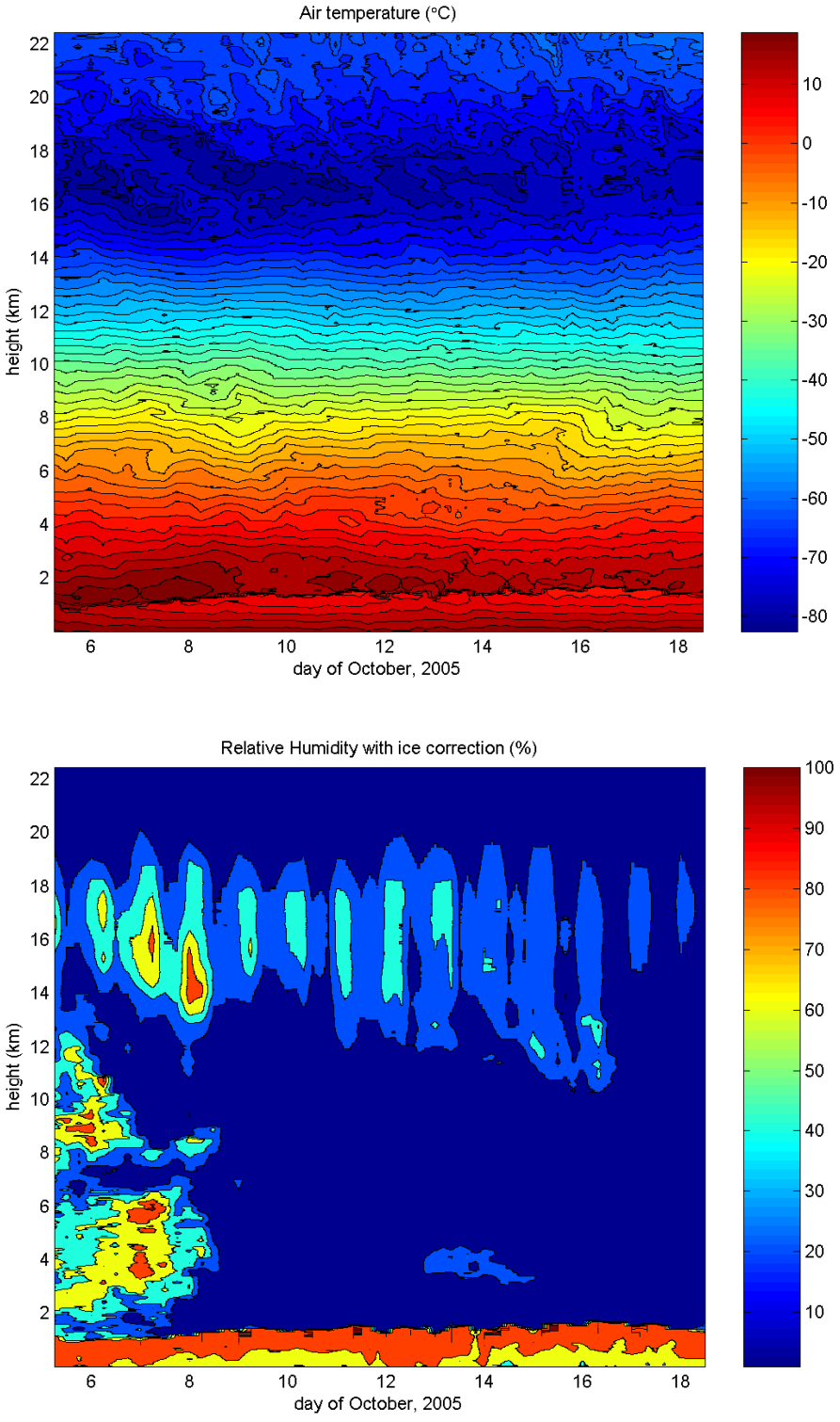

Figure 23. Time-height color contour plots from rawinsondes launched during the 2005 stratus cruise. The upper panel is temperature; the lower panel is relative humidity.

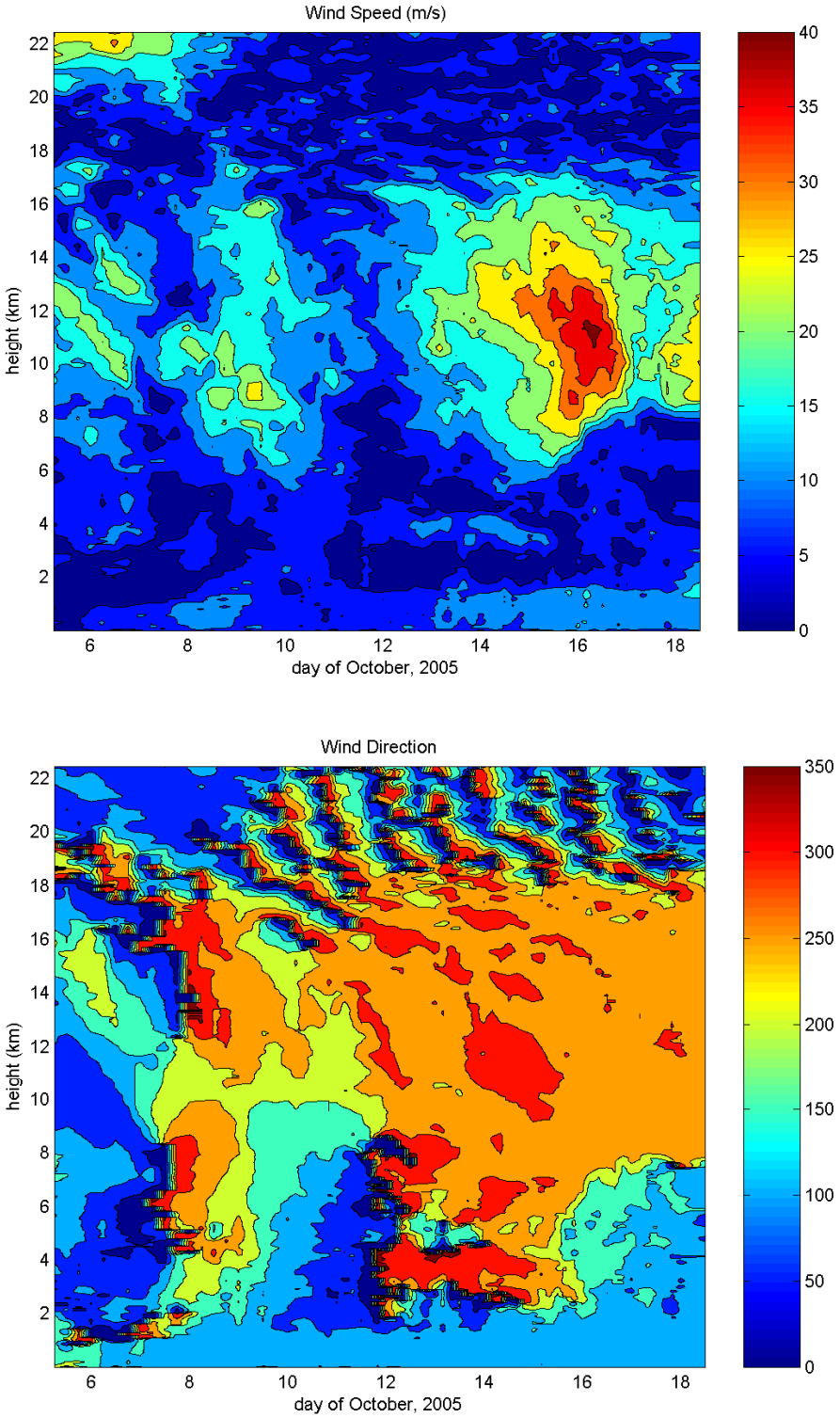

Figure 24. Time-height color contour plots from rawinsondes launched during the 2005 Stratus cruise. The upper panel is wind speed; the lower panel is wind direction.

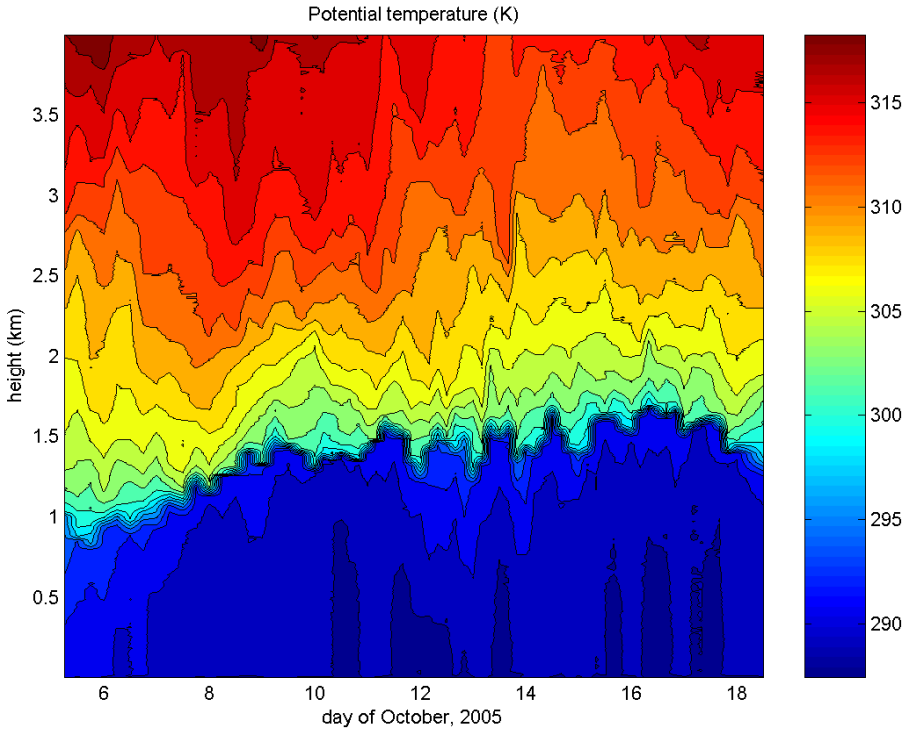

Figure 25. Time-height color contour plots of potential temperature from rawinsondes launched during the 2005 Stratus cruise. This height scale emphasizes the atmospheric boundary layer.

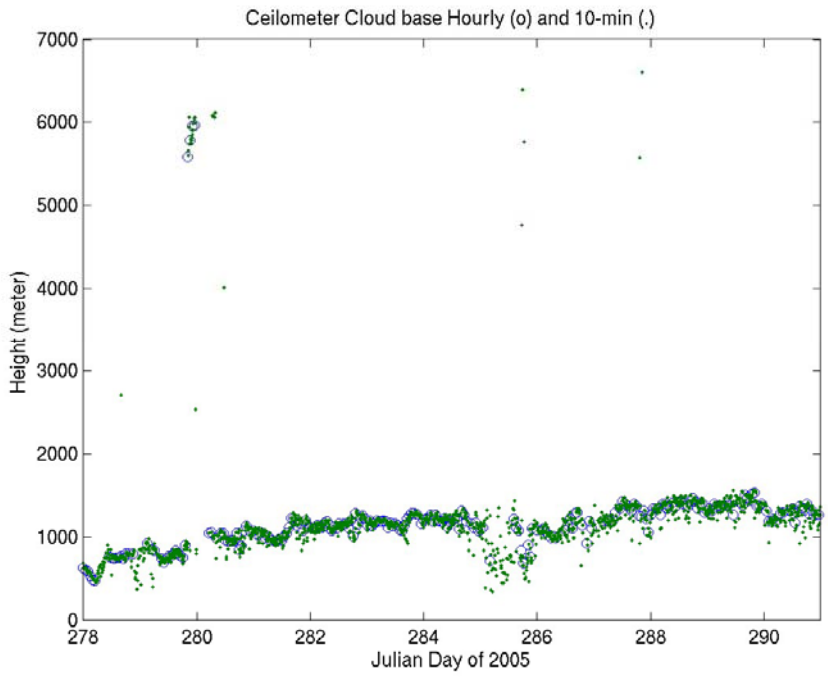

Figure 26. Time series of low cloud-base heights for the experimental period during October.

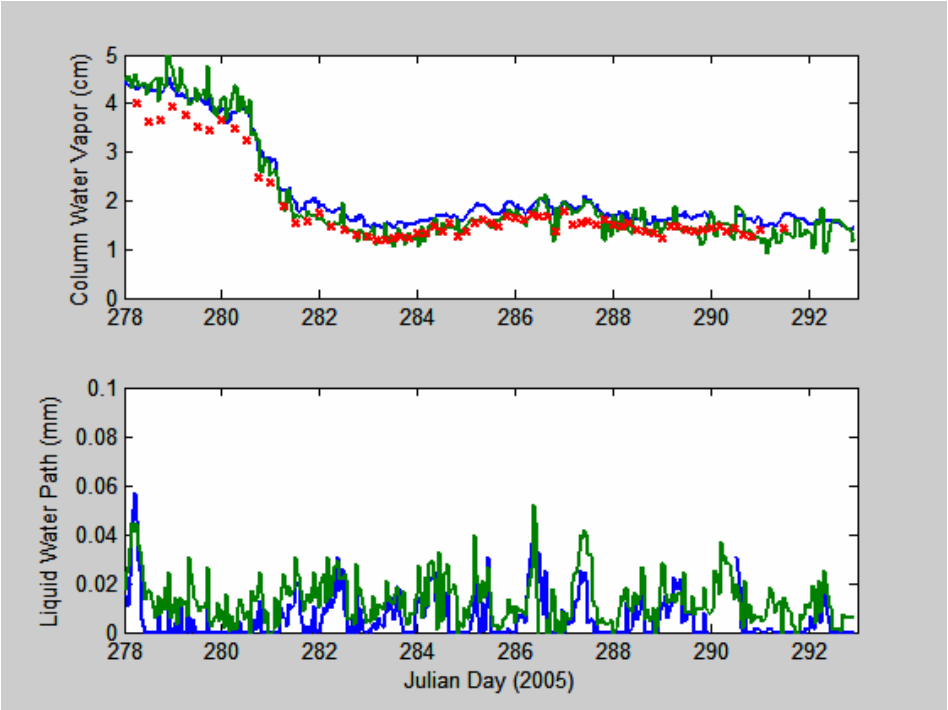

Figure 27. Time series of microwave radiometer-derived values for column integrated water vapor (upper panel) and column integrated liquid water (lower panel). Old mailbox=green, new mailbox=blue, and integrals from rawinsondes profiles=red x's (upper panel only).

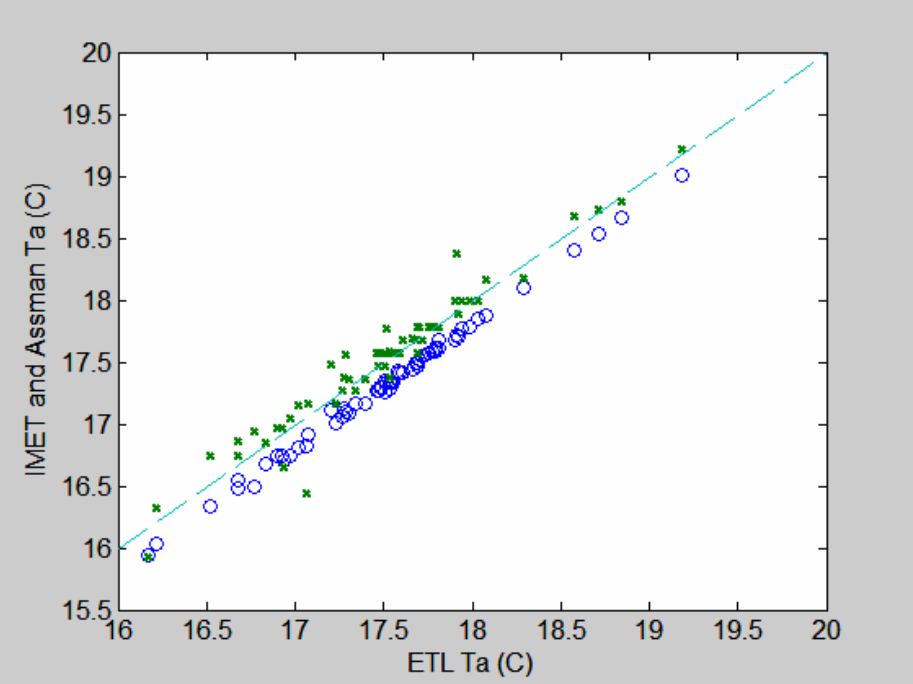

Figure 28. Comparison of simultaneous Assman psychrometer (x's) and ship (circles) readings for air temperature. Psychrometer values corrected to 15 m (ETL and ship instrument height).

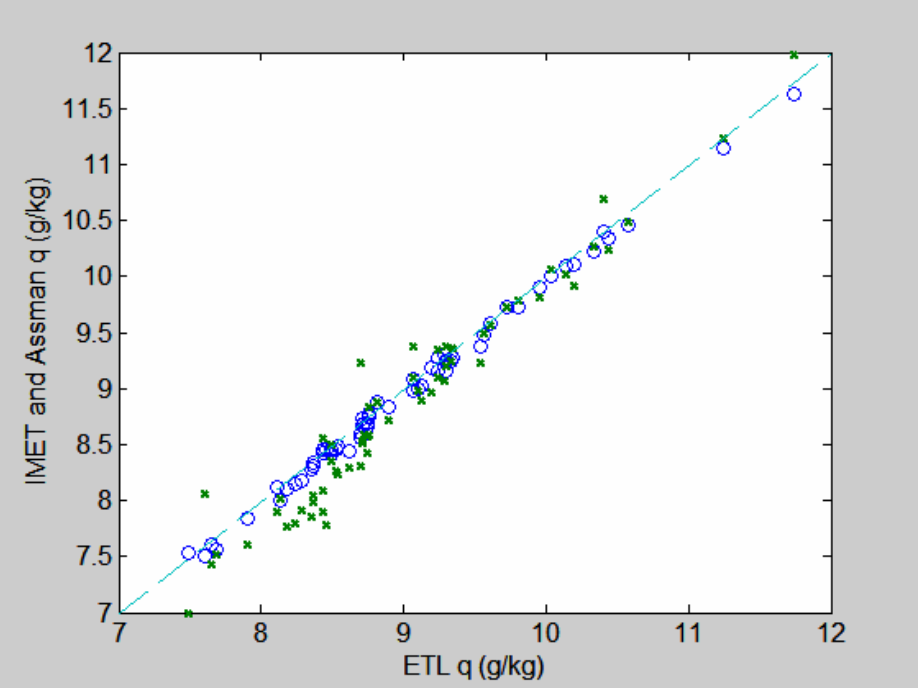

Figure 29. Comparison of simultaneous Assman psychrometer (x's) and ship (circles) readings for specific humidity. Psychrometer values corrected to 15 m (ETL and ship instrument height).